Escuela de
Ingeniería y Arquitectura
Universidad Zaragoza

Trabajo Fin de Máster

Máster en Mecánica Aplicada

Programa Oficial de Posgrado en Mecánica Computacional

Curso 2010-2011

Finite Element study of the angiogenesis process: application to wound healing.

Clara Valero Lázaro

Septiembre de 2011

Directora: Dra. Mª José Gómez Benito
Co-Directora: Dra. Etelvina Javierre Pérez

Departamento de Ingeniería Mecánica
Escuela de Ingeniería y Arquitectura
Universidad de Zaragoza

Finite Element study of the angiogénesis process: application to wound healing.

Resumen

Este trabajo se ha desarrollado en el departamento de Ingeniería Mecánica y su principal objetivo ha sido el desarrollo e implementación de un modelo multifísico del proceso de angiogenesis.

La piel es el órgano más grande del cuerpo humano, encargada del mantenimiento de la integridad de los órganos en su interior. Es de gran importancia su capacidad de autorregeneración ante lesiones. Dadas las particularidades de cada herida y con el fin de obtener el resultado deseado con la mayor eficiencia, deben plantearse tratamientos específicos para cada situación. Para ello, será de gran importancia disponer de técnicas numéricas de simulación que permitan una evaluación rápida de cada caso.

El proceso de cicatrización de heridas se produce en tres etapas: inflamación, proliferación y remodelación. Dentro de la fase de proliferación tienen lugar numerosos procesos, entre ellos la angiogenesis. El proceso de angiogenesis consiste en la formación de vasos sanguíneos a partir de vasos ya existentes. Tras producirse una herida los vasos sanguíneos localizados en el tejido dañado quedan cortados, de manera que se impide la correcta distribución de oxígeno y nutrientes. Por ello es de gran importancia conocer en qué medida afectan los factores presentes en la evolución del proceso de cicatrización. Durante este proceso además se produce una contracción de la herida debida a las tensiones que ejercen las células presentes, tanto en la herida como en la piel que la rodea. Este proceso es el objeto de estudio de este trabajo y depende tanto de las propiedades mecánicas como de las biológicas y químicas de la piel.

En este trabajo se ha implementado en primer lugar un modelo que incluye solo los factores bioquímicos que afectan al proceso de angiogénesis y en segundo lugar un modelo que tiene en cuenta tanto los factores mecánicos como los biológicos para simular el proceso de angiogénesis en la cicatrización de heridas en la piel. Para ello se partió de un modelo matemático de comportamiento de todos los elementos presentes tanto en la herida como en la piel sana, y se evaluó utilizando el Método de los Elementos Finitos (MEF).

Por último, se han comparado los resultados obtenidos con los dos modelos. Para ello se ha prestado atención principalmente a la influencia del oxígeno en el proceso y al efecto de las tensiones mecánicas creadas por las células en las concentraciones de las especies presentes. También se ha estudiado la diferencia en la geometría final de la herida de los dos modelos.

Table of contents

List of figures

List of tables

Chapter 1

Introduction

1.1. Angiogenesis in wound healing

Skin is the largest organ in human body, it covers the whole external body surface and constitutes about the 8 % of the human body mass [14]. Skin has a critical function in maintaining the integrity of the internal organs under it and in preventing the transmission of infections and dehydration. It is equally important its autoregenerative capacity after an injury, getting a perfect healing in almost every case. Skin is an elastic tissue that can be stretched and compressed under certain limits.

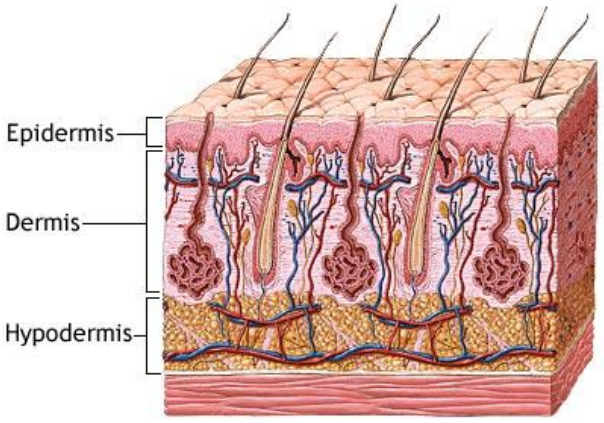

Figure 1.1: *Scheme of the skin layers. ADAM, http://www.adam.com*

Skin consist of various tissue layers (Figure 1.1): the epidermis, the dermis and the hypodermis, and can reach a thickness of 1,5 mm to 4 mm depending on the body part [14]. When important injuries occur in the skin, damage can reach the dermis and the hypodermis, and wound healing is more difficult. The dermis is an irregular connective soft tissue, with a collagen fiber matrix. In this matrix are also allocated nerves, blood vessels and several cellular species. From a mechanical point of view, due to the number and location of the collagen fibers, dermis provides to the skin a high resistance to traction and also a high ability to contract elastically.

Wounds in dermis can appear as a result from surgery or from a traumatic accident. In both cases, a successful healing is crucial for a perfect functional and aesthetic recovery. However, in some situations an optimal healing without an appropriate medical treatment is not possible. Understanding the wound healing process and all the involved factors that influence it is crucial to cure these wounds, in special the complicated ones. Thus, it is very important to understand the mechanical behaviour of the skin against aggressions such as wounds and burns, and its capacity to recover the properties of the undamaged tissue in the shortest time possible.

Wound healing is a natural process in which human body has to regenerate all the skin layers that have suffered damage. During the tissue recovery process, several complex biochemical processes take place to repair the damage. This phenomena overlap in time and can be divided in three stages: inflammatory, proliferative and remodelling, as can be seen in Figure 1.2.

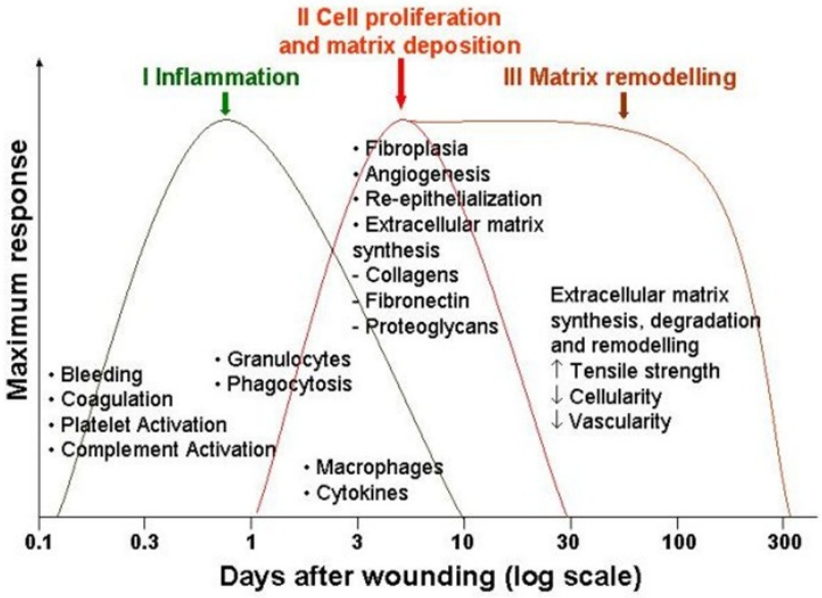

Figure 1.2: *Scheme of the wound healing phases in time.*

After the wound formation both sides of the wound contract towards the centre of the wound, creating mechanical stresses in the skin and inducing the inflammatory respond that initiates the healing process. In the inflammatory phase bacteria are removed and factors that are present in the proliferative stage are released. After that, several phenomena take place in the proliferative phase: angiogenesis, granulation tissue formation, epitheliazation and wound contraction. In this stage new blood vessels and extra cellular matrix (ECM) are created while the wound reduces its size. In the final stage, the collagen fibers are remodelled and realigned and cells that are no needed are removed.

Angiogenesis involves the formation of new blood vessels from the pre-existing vasculature, where capillaries are formed in response to biochemical and mechanical (external) stimuli.

As angiogenesis is present in the wound healing process, it takes place during the second phase (the proliferative stage), it is very important to understand how every factor present in angiogenesis affects the evolution of the wound. When a wound occurs, blood vessels are cut and the wound site is full of blood. To supply the necessary blood and nutrients to the tissue again, the growth or the repair of the blood vessels is crucial. At the beginning of the inflammatory phase cells migrate into the wound site and release angiogenic growth factors [13] that stimulate capillary growth and collagen deposition. This process depends on the biological and chemical species that are present in the skin and the wound.

In addition, these species cause the appearance of mechanical stresses in the tissue. Cells like fibroblasts, have an actomyosin machinery that regulates these stresses depending on the volumetric strain of the surrounding tissue [9]. Therefore, the evolution of the process depends also on the mechanical properties of the skin.

The complexity to obtain experimental data of capillary growth makes more important its research from an *in silico* perspective. Moreover, the social and economic impact of the wound healing process and the vascular growth process makes this field even more important. It shall be mentioned here that angiogenesis is also present in other complex biological phenomena such as bone tissue reconstruction [2], embryogenesis and tumour growth. Hence, the work presented here is relevant and applicable to other important pathologies.

1.2. Angiogenesis models

During the last years a number of mathematical models have been proposed to simulate and reproduce the vascular growth. Maggelakis [7] developed a three variable model that relates the production of macrophage-derived growth factors (MDGF), with the capillary density and the tissue oxygen concentration in one dimension. This model suggests that the healing of a circular wound depends on the oxygen supply. Javierre et al. [4] modified this model, adding a new variable, the epidermal growth factor (EGF) concentration. They propose a coupling between angiogenesis and a wound moving interface due to cell migration in two dimensions.

A different line of models was developed by Pettet et al. [10]. This model has three variables (capillary-tip endothelial cells, macrophage-derived chemoattractants and the new blood vessels) and it is composed by a number of differential equations that describe its behaviour. Later, this model was expanded adding the influence of fibroblasts, oxygen and extracellular matrix [11]. Schugart et al. [13], proposed another model with seven variables that relates the angiogenesis process with the tissue oxygen tension.

1.3. Objectives

The main purpose of this work is the development and implementation of a numerical model that allows to simulate the angiogenesis process in the skin, that takes place during the wound healing process. We will study the influence of biochemical and mechanical factors and this model will be used for two dimensional wounds.

The aim of this work is to go a step forward to obtain a complete model of the wound healing process incorporating all the phases (inflammation, proliferation and angiogenesis, contraction and remodelling)

The work is organised as follows. In first place we have developed a biochemical model of the angiogenesis process, which is presented in Chapter 2. The equations that compose the model are presented together with the results obtained for several geometries. Chapter 3 deals with the mechanical behaviour of the skin and the wound and how this behaviour can influence the angiogenesis process. We propose the coupling of the biochemical model with a hyperelastic model for the mechanical skin behaviour. In this chapter, the results of the whole model are presented for several different geometries and we compare the results obtained here with the ones just considering biochemical factors from Chapter 2. Finally, Chapter 4 presents the conclusions of this work and the future lines to continue the investigation.

Chapter 2

Biochemical model of angiogenesis

As it has been previously said (Chapter 1), a number of mathematical and numerical angiogenesis models have been developed during the last few years. Angiogenesis is present in the second stage of the wound healing process, the proliferative phase, so it is very important to understand how every factor present in this process affects the evolution of the wound.

In this work, we propose a continuous angiogenesis model that incorporates biological and chemical factors, consisting of a number of coupled reaction-diffusion equations. The primary variables of the model are the concentrations of oxygen (u_1), macrophage-derived growth factors -such as VEGF (vascular endothelial growth factor) or others, henceforth MDGF- (u_2), capillary density (u_3) and fibroblasts (n). We have modified the model proposed by Javierre et al. [4], based on the model of Maggelakis [7], in order to introduce the effect of fibroblasts in the process. The main advance of this model with respect to the one of Javierre et al. [4] is the replacement of the EGF (epidermal growth factor) with the fibroblasts since this model will be coupled with a previous model of the contraction phase, which is regulated by the fibroblasts density. The aim of this work is to move forward a more complete model of the wound healing process incorporating all the phases (inflamation, proliferation and angiogenesis, contraction and remodeling)

In the next section we present the set of equations that describes the behaviour of the variables. These equations represent a volumetric conservation law for every species.

2.1. Conservation of species

We propose a different conservation law for every species that includes the most important mechanisms of variation of the species concentrations: production, transport and decay.

2.1.1. Oxygen (u_1)

Oxygen is required for wound healing and in the angiogenesis process. Low levels of oxygen impairs the healing process [12] since reparative processes such as cell proliferation and angiogenesis require a high oxygen demand. It is assumed that the oxygen flux is due to

diffusion, it is supplied by the capillary vasculature [13] and its own consumption is due to chemical decay. The resulting equation for the oxygen variation is

$$\frac{\partial u_1}{\partial t} = D_1 \nabla^2 u_1 + \lambda_{3,1} u_3 - \lambda_{1,1} u_1 \tag{2.1}$$

where D_1 is the diffusion parameter, $\lambda_{3,1}$ is the oxygen production rate caused by the capillaries and $\lambda_{1,1}$ is the oxygen decay rate.

2.1.2. Macrophage-derived growth factor (MDGF) (u_2)

Macrophages appear at the wound site when the concentration of oxygen is at low levels. Macrophages release chemical substances, MDGFs, that stimulate vessel growth (to increase the oxygen concentration) and collagen deposition. The flux of MDGF is due to diffusion, with a diffusion coefficient D_2, and its production depends on the oxygen density and its consumption is due to chemical decay. The equation for the MDGF is

$$\frac{\partial u_2}{\partial t} = D_2 \nabla^2 u_2 + \lambda_{1,2} P(u_1) - \lambda_{2,2} u_2 \tag{2.2}$$

where the appearing parameters are included in Table 2.1 and P represents the function describing the production of MDGF when the levels of oxygen are low,

$$P(u_1) = \begin{cases} 1 - \frac{u_1}{u_1^{\beta_2}} & if \quad u_1 < u_1^{\beta_2}; \\ 0 & otherwise \end{cases} \tag{2.3}$$

and $u_1^{\beta_2}$ is the oxygen concentration below which MDGFs are produced.

2.1.3. Capillary density (u_3)

Capillaries are the smallest blood vessels and are part of the microcirculation system. They are in charge of supplying nutrients and oxygen to the tissue. When a wound occurs capillaries are cut and its recovery is crucial for the correct wound healing. It is assumed that capillary cells undergo migration, which is modelled as a random diffusion following Fick‘s law, and are also produced according to a logistic model with growth rate proportional to the MDGF density. High levels of MDGF activate capillary growth and when the capillary density is high, near the maximal possible concentration, their growth is inhibited [7]. The equation for the capillary density is

$$\frac{\partial u_3}{\partial t} = D_3 \nabla^2 u_3 + \lambda_{3,2} u_2 u_3 (1 - \frac{u_3}{u_3^{eq}}) \tag{2.4}$$

where u_3^{eq} is the maximal capillary density in the undamaged skin.

2.1.4. Fibroblasts (n)

Fibroblasts are motile cells that can exert traction forces on the surrounding tissue. It is known that fibroblasts are responsible of ECM synthesis, and serve as an indicator of ECM maturity. Hence, as a novelty from the previous model [4], we have incorporated the fibroblasts equation (Eq. (2.5)) in which fibroblast proliferation is modelled with a logistic

term with oxygen dependent rate [13]. Moreover, the fibroblasts flux is due to migration modelled as a random diffusion (random dispersal), whereas fibroblasts net production is due to cell proliferation and death. Therefore, the fibroblasts governing equation can be written as

$$\frac{\partial n}{\partial t} = D_n \nabla^2 u_n - \lambda_{n,n} n + r_n n(1 - \frac{n}{K}) u_1 (1 - \frac{u_1}{K_1}). \tag{2.5}$$

The description and values of the normalised model parameters are included in Table 2.1. The values have been estimated or taken from the literature [4] [5] when is possible.

Parameter	Description	Dimensionless value
D_1	Oxygen diffusion rate	$4.32{\cdot}10^{-3}$
$\lambda_{3,1}$	Oxygen production rate caused by the capillary	0.864
$\lambda_{1,1}$	Oxygen consumption rate	0.864
D_2	MDGF diffusion rate	0.0864
$\lambda_{1,2}$	MDGF production rate in hypoxia state	2.592
$\lambda_{2,2}$	MDGF death rate	0.864
D_3	Capillary diffusion rate	$4.32{\cdot}10^{-3}$
$\lambda_{3,2}$	Capillary production rate	43.2
u_3^{eq}	Maximal capillary density	1.0
D_n	Fibroblasts diffusion rate	$2{\cdot}10^{-2}$
$\lambda_{n,n}$	Fibroblasts death rate	0.7488
r_n	Maximal rate of fibroblasts proliferation	0.832
K	Fibroblasts maximal capacity in dermis	10.0
K_1	Oxygen concentration above which MDGFs do not induce vascular growth	5000.0
$u_1^{\beta_2}$	Oxygen concentration below which MDGFs are produced	0.25

Table 2.1: List of normalised model parameters related to the biochemical model.

2.2. Numerical implementation of the biochemical model

From the mathematical model presented in Section 2.1 we have developed a numerical model to simulate the angiogenesis process in two-dimensional wounds. This model has been implemented through an Abaqus user subroutine. We have solved the resulting problem using a finite element analysis. Finite Element Method (FEM) was chosen as it adapts to complex geometries, feature that is needed to simulate the wound shapes. The primary unknowns (u_1, u_2, u_3, n) are interpolated from nodal values through shape functions ($\mathbf{N}$) and the time derivatives are approximated with a generalised trapezoidal method [3]. The resulting nonlinear system of equations is solved using a standard Newton-Raphson method.

To obtain the complete coupled non-linear system of equations, that describes the discrete model, we obtain first the weak formulation of the governing equations. For this, we use the Gauss' theorem under the assumption of sufficient differentiability. To obtain the weak formulation we take into account the boundary conditions of the primary unknowns, that determine the space of admissible solutions.

2.2.1. System of equations nonlinearly coupled

The model primary unknowns can be written in function of their nodal values through their associated shape functions [16]. For a general species Q, where $\mathbf{x}$ are the node coordinates in a time t, the expresion is as follows

$$Q^h(\mathbf{x},t) = \mathbf{N}_Q(\mathbf{x})\mathbf{Q}(t), \tag{2.6}$$

where $\mathbf{Q}$ is a vector that comprises the primary unknowns species(u_1, u_2, u_3, n) and the superscript h denotes the finite element solution and $\mathbf{N}_{(*)}(\mathbf{x})$ the shape functions. To reach the algebraic discrete and non-linear system of equations, these approximations are substituted in the weak formulation, choosing the weighting functions equal to the shape functions. The nodal values of the primary time-dependant unknowns can be obtained from the resulting system of equations. This system can be expressed as a balance of internal and external forces:

$$\mathbb{F}\big(\mathbb{Z}_{n+1}\big) := \mathbb{F}^{int}\big(\mathbb{Z}_{n+1}\big) - \mathbb{F}^{ext}\big(\mathbb{Z}_{n+1}\big) = \mathbf{0}, \tag{2.7}$$

where $\mathbb{Z}$ comprises the time-dependent nodal values of the primary variables, expressed as

$$\mathbb{Z} = \big(\mathbf{u_1}^T\ \mathbf{u_2}^T\ \boldsymbol{u_3}^T\ \mathbf{n}^T\big)^T \tag{2.8}$$

and the superscript $(n+1)$ represents the time step where the solution is being calculated. The internal and external forces $\mathbb{F}^{int}$ and $\mathbb{F}^{ext}$ can be represented in a vectorial form

$$\mathbb{F}^{int} = \Big[(\mathbf{F}^{int}_{u_1})^T\ (\mathbf{F}^{int}_{u_2})^T\ (\mathbf{F}^{int}_{u_3})^T\ (\mathbf{F}^{int}_{n})^T\Big]^T, \tag{2.9}$$

$$\mathbb{F}^{ext} = \Big[(\mathbf{F}^{ext}_{u_1})^T\ (\mathbf{F}^{ext}_{u_2})^T\ (\mathbf{F}^{ext}_{u_3})^T\ (\mathbf{F}^{ext}_{n})^T\Big]^T, \tag{2.10}$$

where

$$\mathbf{F}^{int}_{u_1} = \int_\Omega \mathbf{N}^T_{u_1}\frac{\partial u_1}{\partial t}\,d\Omega + \int_\Omega \nabla\mathbf{N}^T_{u_1} D_1 \nabla u_1 d\Omega \tag{2.11}$$

$$\mathbf{F}^{int}_{u_2} = \int_\Omega \mathbf{N}^T_{u_2}\frac{\partial u_2}{\partial t}d\Omega + \int_\Omega \nabla\mathbf{N}^T_{u_2} D_2 \nabla u_2 d\Omega \tag{2.12}$$

$$\mathbf{F}^{int}_{u_3} = \int_\Omega \mathbf{N}^T_{u_3}\frac{\partial u_3}{\partial t}\,d\Omega + \int_\Omega \nabla\mathbf{N}^T_{u_3} D_3 \nabla u_3 d\Omega \tag{2.13}$$

$$\mathbf{F}^{int}_{n} = \int_\Omega \mathbf{N}^T_{n}\frac{\partial n}{\partial t}\,d\Omega + \int_\Omega \nabla\mathbf{N}^T_{n} D_n \nabla n d\Omega \tag{2.14}$$

$$\mathbf{F}^{ext}_{u_1} = \int_\Omega \mathbf{N}^T_{u_1}\lambda_{3,1}u_3 d\Omega - \int_\Omega \mathbf{N}^T_{u_1}\lambda_{1,1}u_1 d\Omega \tag{2.15}$$

$$\mathbf{F}^{ext}_{u_2} = \int_\Omega \mathbf{N}^T_{u_2}\lambda_{2,1}\big(1-\frac{u_1}{u_1^{\theta_2}}\big)d\Omega - \int_\Omega \mathbf{N}^T_{u_2}\lambda_{2,2}u_2 d\Omega \tag{2.16}$$

$$\mathbf{F}^{ext}_{u_3} = \int_\Omega \mathbf{N}^T_{u_3}\Big(1-\frac{u_3}{u_3^e q}\Big)u_2 u_3 d\Omega \tag{2.17}$$

$$\mathbf{F}^{ext}_{n} = \int_\Omega -\mathbf{N}^T_{n}\lambda_{n,n} n d\Omega - \int_\Omega r_n n \mathbf{N}^T_n\Big(1-\frac{n}{K}\Big)u_1\Big(1-\frac{u_1}{K_1}\Big)d\Omega \tag{2.18}$$

where, working with two-dimensional geometries and being $\mathbf{N}_{(*)}(\mathbf{x})$ the shape functions in the nodes and nnod the total number of nodes, the matrices in the problem have the form

$$\mathbf{N}_{u_1} = \begin{pmatrix} \mathbf{N}^1_{u_1} & \mathbf{N}^2_{u_1} & \cdots & \mathbf{N}^{nnod}_{u_1} \end{pmatrix}$$

$$\mathbf{N}_{u_2} = \begin{pmatrix} \mathbf{N}^1_{u_2} & \mathbf{N}^2_{u_2} & \cdots & \mathbf{N}^{nnod}_{u_2} \end{pmatrix}$$

$$\mathbf{N}_{u_3} = \begin{pmatrix} \mathbf{N}^1_{u_3} & \mathbf{N}^2_{u_3} & \cdots & \mathbf{N}^{nnod}_{u_3} \end{pmatrix}$$

$$\mathbf{N}_{n} = \begin{pmatrix} \mathbf{N}^1_{n} & \mathbf{N}^2_{n} & \cdots & \mathbf{N}^{nnod}_{n} \end{pmatrix}$$

$$\nabla\mathbf{N}_{u_1} = \begin{pmatrix} \frac{\partial \mathbf{N}^1_{u_1}}{\partial x} & & \frac{\partial \mathbf{N}^{nnod}_{u_1}}{\partial x} \\ \frac{\partial \mathbf{N}^1_{u_1}}{\partial y} & \cdots & \frac{\partial \mathbf{N}^{nnod}_{u_1}}{\partial y} \end{pmatrix}$$

$$\nabla\mathbf{N}_{u_2} = \begin{pmatrix} \frac{\partial \mathbf{N}^1_{u_2}}{\partial x} & & \frac{\partial \mathbf{N}^{nnod}_{u_2}}{\partial x} \\ \frac{\partial \mathbf{N}^1_{u_2}}{\partial y} & \cdots & \frac{\partial \mathbf{N}^{nnod}_{u_2}}{\partial y} \end{pmatrix}$$

$$\nabla\mathbf{N}_{u_3} = \begin{pmatrix} \frac{\partial \mathbf{N}^1_{u_3}}{\partial x} & & \frac{\partial \mathbf{N}^{nnod}_{u_3}}{\partial x} \\ \frac{\partial \mathbf{N}^1_{u_3}}{\partial y} & \cdots & \frac{\partial \mathbf{N}^{nnod}_{u_3}}{\partial y} \end{pmatrix}$$

$$\nabla\mathbf{N}_{n} = \begin{pmatrix} \frac{\partial \mathbf{N}^1_{n}}{\partial x} & & \frac{\partial \mathbf{N}^{nnod}_{n}}{\partial x} \\ \frac{\partial \mathbf{N}^1_{n}}{\partial y} & \cdots & \frac{\partial \mathbf{N}^{nnod}_{n}}{\partial y} \end{pmatrix}$$

The solution of the nonlinear system of equations can be obtained applying a standard Newton-Raphson method [16].

2.2.2. Jacobian matrices of the internal and external forces

The Jacobian matrices corresponding to the internal and external forces with non-zero value resulting from the system of equations are now presented. In the used notation, α represents the characteristic temporal parameter of the trapezoidal integration method. The non-zero terms of the Jacobian matrices $\partial\mathbb{F}^{int}/\partial\mathbb{Z}$ and $\partial\mathbb{F}^{ext}/\partial\mathbb{Z}$ are:

$$\frac{\partial \mathbf{F}_{u_1}^{int}}{\partial \mathbf{u_1}} = \frac{1}{\alpha \Delta t} \int_\Omega \mathbf{N}_{u_1}^T \mathbf{N}_{u_1} d\Omega + \int_\Omega \nabla \mathbf{N}_{u_1}^T D_1 \nabla \mathbf{N}_{u_1} d\Omega \tag{2.19}$$

$$\frac{\partial \mathbf{F}_{u_2}^{int}}{\partial \mathbf{u_2}} = \frac{1}{\alpha \Delta t} \int_\Omega \mathbf{N}_{u_2}^T \mathbf{N}_{u_2} d\Omega + \int_\Omega \nabla \mathbf{N}_{u_2}^T D_2 \nabla \mathbf{N}_{u_2} d\Omega \tag{2.20}$$

$$\frac{\partial \mathbf{F}_{u_3}^{int}}{\partial \mathbf{u_3}} = \frac{1}{\alpha \Delta t} \int_\Omega \mathbf{N}_{u_3}^T \mathbf{N}_{u_3} d\Omega + \int_\Omega \nabla \mathbf{N}_{u_3}^T D_3 \nabla \mathbf{N}_{u_3} d\Omega \tag{2.21}$$

$$\frac{\partial \mathbf{F}_{n}^{int}}{\partial \mathbf{n}} = \frac{1}{\alpha \Delta t} \int_\Omega \mathbf{N}_{n}^T \mathbf{N}_{n} d\Omega + \int_\Omega \nabla \mathbf{N}_{n}^T D_n \nabla \mathbf{N}_{n} d\Omega \tag{2.22}$$

$$\frac{\partial \mathbf{F}_{u_1}^{ext}}{\partial \mathbf{u_1}} = -\int_\Omega \mathbf{N}_{u_1}^T \mathbf{N}_{u_1} \lambda_{1,1} d\Omega \tag{2.23}$$

$$\frac{\partial \mathbf{F}_{u_1}^{ext}}{\partial \mathbf{u_3}} = \int_\Omega \mathbf{N}_{u_1}^T \mathbf{N}_{u_3} \lambda_{3,1} d\Omega \tag{2.24}$$

$$\frac{\partial \mathbf{F}_{u_2}^{ext}}{\partial \mathbf{u_1}} = \int_\Omega \mathbf{N}_{u_2}^T \mathbf{N}_{u_1} \lambda_{2,1} \big(\frac{-1}{u_1^{\theta_2}}\big) d\Omega \tag{2.25}$$

$$\frac{\partial \mathbf{F}_{u_2}^{ext}}{\partial \mathbf{u_2}} = -\int_\Omega \mathbf{N}_{u_2}^T \mathbf{N}_{u_2} \lambda_{2,2} d\Omega \tag{2.26}$$

$$\frac{\partial \mathbf{F}_{u_3}^{ext}}{\partial \mathbf{u_2}} = \int_\Omega \mathbf{N}_{u_3}^T \mathbf{N}_{u_2} \lambda_{3,2} u_3 \big(1 - \frac{u_3}{u_3^{eq}}\big) d\Omega \tag{2.27}$$

$$\frac{\partial \mathbf{F}_{u_3}^{ext}}{\partial \mathbf{u_3}} = -\int_\Omega \mathbf{N}_{u_3}^T \mathbf{N}_{u_3} \lambda_{3,2} u_2 \big(1 - \frac{2u_3}{u_3^{eq}}\big) d\Omega \tag{2.28}$$

$$\frac{\partial \mathbf{F}_{n}^{ext}}{\partial \mathbf{n}} = -\int_\Omega \mathbf{N}_{n}^T \mathbf{N}_{n} \lambda_{n,n} d\Omega + \int_\Omega r_n \mathbf{N}_{n}^T \mathbf{N}_{n} u_1 \big(1 - \frac{2n}{K}\big)\big(1 - \frac{u_1}{K_1}\big) d\Omega \tag{2.29}$$

$$\frac{\partial \mathbf{F}_{n}^{ext}}{\partial \mathbf{u_1}} = \int_\Omega r_n \mathbf{N}_{n}^T \mathbf{N}_{u_1} n \big(1 - \frac{n}{K}\big)\big(1 - \frac{2u_1}{K_1}\big) d\Omega \tag{2.30}$$

From these expressions it is possible to obtain the necessary block matrices to assembly the global stiffness matrix.

2.3. Initial and boundary conditions

The computational domain Ω consists of two disjoint parts: the wound Ω_w and the undamaged surrounding tissue Ω_{und} (see Figure 2.1).

As initial conditions we have considered that the initial concentration of every species is null in the wound site. As a result from the injury, every species are removed from the damaged skin. The undamaged tissue is full of all the species except MDGF (u_2), which is not present. MDGF will appear in the wound site after the initiation of the model, due to the low oxygen concentration.

As boundary conditions we have considered that the domain is sufficiently large in order to prescribe null fluxes through the frontier and no displacements at the boundary.

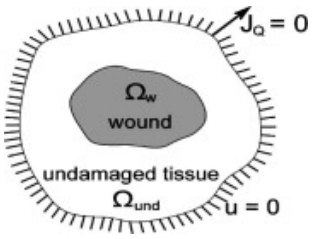

Figure 2.1: *Computational domain of the 2D problem.*

2.4. Numerical results of the biochemical model

In a first approach, a circular wound has been studied. The diameter of the wound is 2 cm and it is surrounded by a 10 cm diameter circumference of undamaged skin. We have simulated a fourth of the whole geometry as we have considered symmetry in the two axes.

2.4.1. Evolution of the species in the wound centre

We analyse the results in the centre of the wound, which is the furthest point to the undamaged skin and supposedly the last point to heal. We show the evolution of the species concentration in the wound centre along the simulated time (see Figure 2.2), in this case 30 days where simulated as it was assumed that it is a long enough period for the wound to be completely vascularized.

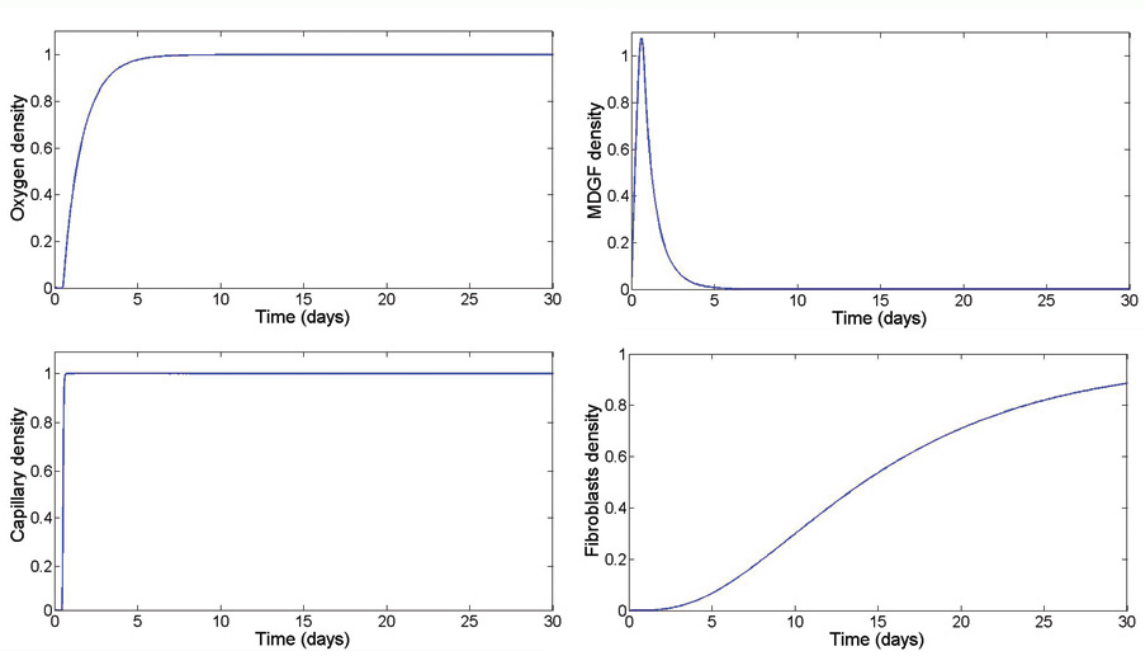

Figure 2.2: *Evolution of the oxygen density (top left), MDGF density (top right), capillary density (bottom left) and fibroblasts density (bottom right) in the centre of the wound during the simulated time.*

We observe how the oxygen concentration regulates the rest of the variables. While there is no oxygen in the centre of the wound the level of MDGF increases rapidly, which

cause the appearance of capillaries. When the capillary density grows, more oxygen is supplied to the wound centre and the MDGF gradually disappears. The capillary density grows rapidly to the capillary density of undamaged tissue (u_3^{eq}) when the oxygen density begins to increase and after that, the fibroblasts density grows indicating that the dermis is being restored.

2.4.2. Oxygen influence

We have studied the effect of oxygen in the fibroblasts behaviour. It is clear from the results that oxygen affects the fibroblasts concentration (see Figure 2.3). When oxygen is not included in the fibroblasts kinetics, the model predicts fibroblasts invasion into the wound faster than reality, and hence wound healing rate is overestimated.

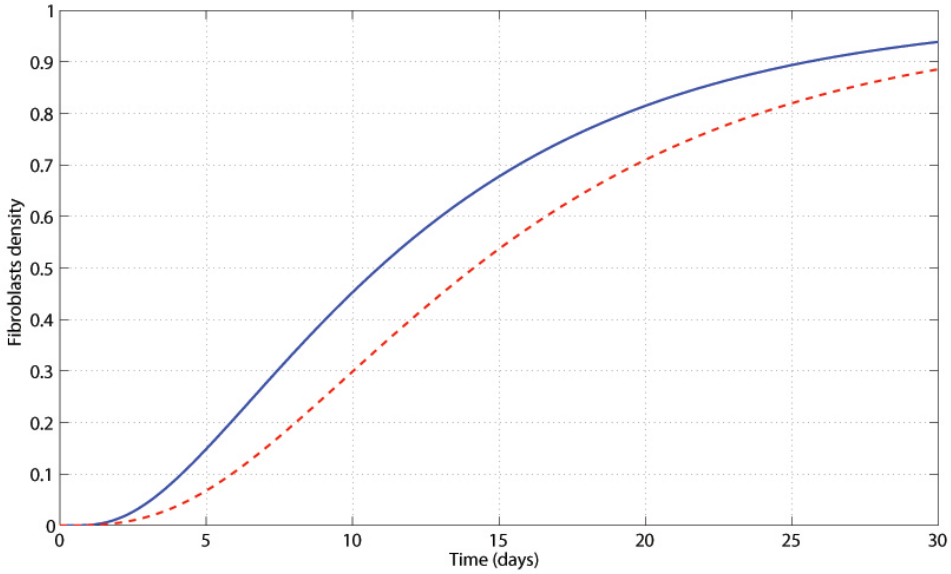

Figure 2.3: *Evolution of the fibroblasts density in the wound centre without the influence of oxygen (continuous line) and the oxygen effect (dashed line.)*

2.4.3. Species density in the whole geometry

To finish this Chapter, we have studied the distribution of every species one day post-wounding. The results are shown in Figure 2.4. Results show an elevated density of MDGF in the wound area, and slowing growing density of oxygen, capillaries and fibroblasts. The advance of the so-called healing unit, with the capillaries in first term followed by the fibroblasts, is visible.

After a few days the concentrations of all the species are homogeneous in the whole domain. Both, oxygen and capillary density reach a concentration of 1 (the normalised density of undamaged dermis), while MDGF appears in the wound site during the first days but then disappears. Finally, the fibroblasts concentration progresses more slowly, but finally reaches the fibroblast density of the undamaged dermis.

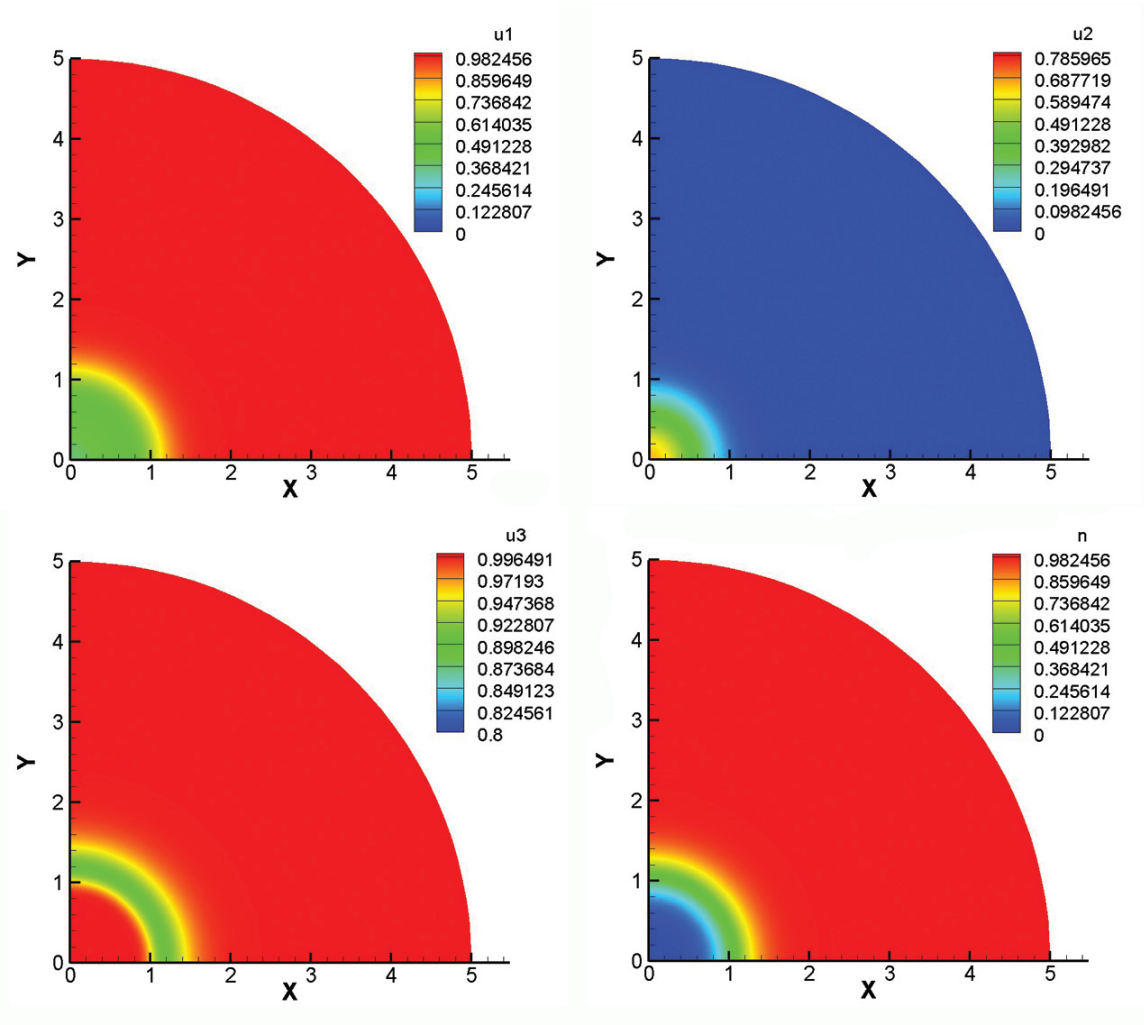

Figure 2.4: *Distribution of oxygen (top left), MDGF (top right), capillary (bottom left) and fibroblasts (bottom right) in the whole domain one day after wounding.*

Chapter 3

Mechanobiochemical model of angiogenesis

As it has been said in Chapter 1, angiogenesis is a biological process but it is not only influenced by biochemical factors, it is also influenced by mechanical stimuli. When mechanical stresses appear in the skin the geometry of the wound is modified and it affects also the evolution of the biochemical process.

In this work, we propose an angigenesis model that includes biological and mechanical factors. For that, we calculate the variation of the biochemical species that are present in the process with the model proposed in Chapter 2 and we have also implemented the mechanical behaviour of the skin and cells. We have implemented this model in a non-coupled way, so we resolve the biochemical equations and the mechanical analysis separately due to the different time scales at which mechanical and biochemical processes occur.

3.1. Mechanosensing model

As it has been previously said, cells (in this model we assume the most important cell type in angiogenesis are fibroblasts) can exert forces in the surrounding tissue where they are allocated. This mechanical behaviour is due to their actomyosin mechanism [9]. From the species densities values we can obtain the net stress of one fibroblasts cell per unit of extra-cellular matrix (ECM), p_{cell}, which, in this work, is considered to be the mechanical stimulus that regulates the forces exerted by cells. Since endothelial cells (which form the capillaries) are active in ECM production, we assume that the ECM density is proportional to the capillary density. We take p_{cell} following Moreo et al. [9]. In their work Moreo et al. proposed an active mechanosensing model based on the Hill's model for skeletal muscle behaviour, applicable to cell-substrate interaction situations. In this work p_{cell} is a piecewise linear function depending on the tissue volumetric strain

$$p_{cell} = \begin{cases} K_{pas}\theta & \theta < \theta_1 \\ \frac{K_{act}p_{max}}{K_{act}\theta_1 - p_{max}}(\theta_1 - \theta) + K_{pas}\theta & \theta_1 \leq \theta \leq \theta^* \\ \frac{K_{act}p_{max}}{K_{act}\theta_2 - p_{max}}(\theta_2 - \theta) + K_{pas}\theta & \theta^* < \theta \leq \theta_2 \\ K_{pas}\theta & \theta > \theta_2 \end{cases} \tag{3.1}$$

where θ^* can be defined as $\theta^* = p_{max}/K_{act}$.

p_{cell} is a mechanosensing variable that depends on the volumetric strain θ of the tissue where cells are allocated. As the cell actomyosin machinery responds actively only between certain limits, we have considered θ_1 and θ_2, which are the compresion and traction strain limits within which the machinery works. p_{max} denotes the maximal contractile force that the actomyosin machinery can exert, and K_{act} and K_{pas} the stiffness moduli of the active and passive components of the cell. The values of these parameters [5] are included in Table 3.1.

Parameter	Description	Dimensionless value
p_{max}	maximal cellular active stress per unit of ECM	1
K_{pas}	volumetric stiffness moduli of the passive components of the cell	$2{\cdot}10^{-1}$
K_{act}	volumetric stiffness moduli of the actin filaments of the cell	1
θ_1	shortening strain of the contractile element	-0.6
θ_2	lengthening strain of the contractile element	0.5
R_τ	traction inhibition collagen density	$5{\cdot}10^{-3}$
K_{ecm}	ECM production rate per unit of capillary density	1

Table 3.1: List of normalised model parameters related to the mechanical behaviour.

p_{cell} and the species densities determine stresses that cells are creating in the surrounding tissue. In this work we have considered that the traction stresses, that are created by punctual forces exerted by cells, can be written as

$$\boldsymbol{\sigma}_{cell} = p_{cell}(\theta)\frac{n\rho_{ecm}}{R_\tau^2 + \rho_{ecm}^2} \tag{3.2}$$

following Javierre et al [5].

Using Equation (3.2), cell traction forces are considered isotropic, generated by fibroblasts and inhibited at high ECM density. In addition, we have considered that the density of the extracellular matrix can be expressed as a function of the capillaries in the skin, thus it is assumed that capillaries can be present only when there is a substrate to stay, in this case the ECM density (ρ_{ecm}) is expressed as,

$$\rho_{ecm} = K_{ecm}u_3, \tag{3.3}$$

where K_{ecm} is a constant.

3.2. Material model of the skin

In the numerous studies where skin is simulated, it has been modelled with different material behaviours. In some of these works, as in Javierre et al. [5], skin is assumed to be viscoelastic and it is characterised by its usual stress-strain constitutive relation. However, other works centered just in the mechanical behaviour of skin [1] [6], assume skin as a hyperelastic material, which is more accurate. Thus, in this work skin has been considered as a hyperelastic material. We have used a second order polynomial strain energy potential model with the form [1]

$$\psi = \sum_{i+j=1}^{2} C_{ij}(\overline{I}_1 - 3)^i(\overline{I}_2 - 3)^j + \sum_{i=1}^{2} \frac{1}{D}(J_{el} - 1)^{2i} \tag{3.4}$$

where ψ is the strain energy per unit of reference volume and $\overline{I}_1$ and $\overline{I}_2$ are the first and second deviatoric invariants. The values of the material parameters C_{ij} and D_i have been taken from previous skin studies [1], where the parameters were calculated for a normal stiffness tissue. The values of the parameters are presented in Table 3.2. As far as we know, there is no work in literature which determine mechanical properties of damaged skin. Thus, in a first approach mechanical properties of the damaged skin were assumed to be the same as the undamaged skin properties.

Parameter	$\mathbf{C_{10}}$	$\mathbf{C_{01}}$	$\mathbf{C_{20}}$	$\mathbf{C_{11}}$	$\mathbf{C_{02}}$	**D**
Value	0.08556	-0.05841	0.03900	-0.02319	0.00851	3.65273

Table 3.2: Values of the hyperelastic parameters. Units are Nmm^2 for C_{ij} and mm^2N^{-1} for D.

3.3. Implementation of the mechanobiochemical model

In this work we have implemented the biochemical and the mechanical behaviour of the skin in the angiogenesis process separately, due to the different time scales at which biochemical and mechanical events occur during wound healing it is assumed more appropriate. However both parts of the model have some variables in common, and these variables are used to merge the biochemical and mechanical parts and close the model. The scheme of the implementation is shown in Figure 3.1

In the biochemical analysis we are evaluating the evolution of the species densities in a fixed geometry, that does not vary in time. The value of these stresses depends on the volumetric strain θ as has been explained in Section 3.1, and at the beginning of the calculation θ is zero as the tissue has not been yet deformed. To solve the problem in this non-coupled way we use an updated Lagrangian formulation, so we work with the deformed coordinates in both biochemical and mechanical analyses.

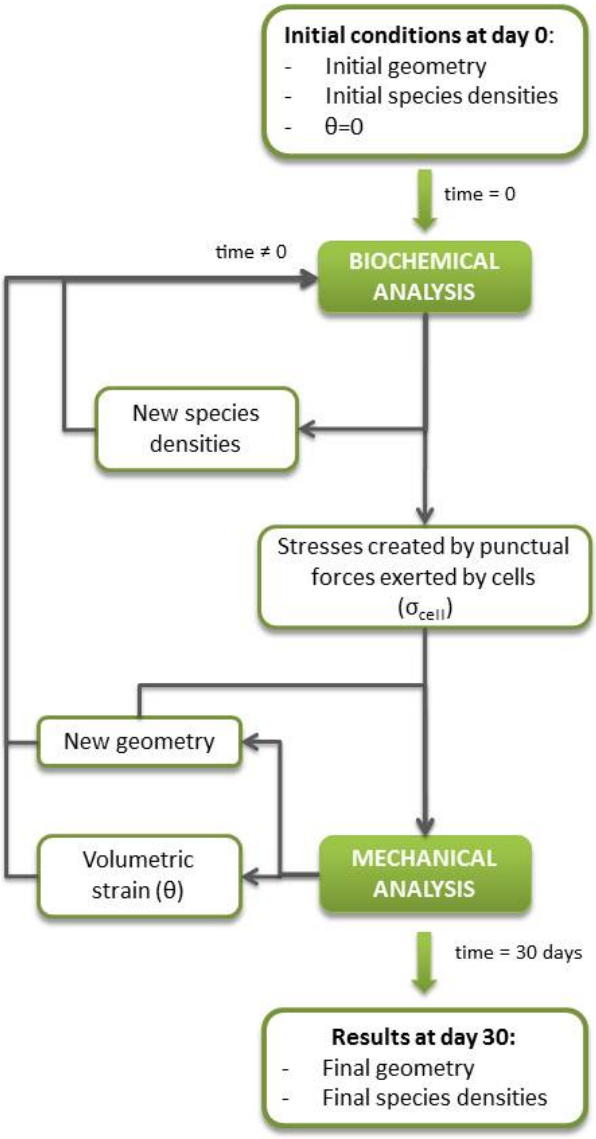

Figure 3.1: *Scheme of the complete model.*

The value of the stresses σ_{cell} (Eq. (3.2)) in every node of the mesh is calculated in the same subroutine used in the biochemical model and introduced in the hyperelastic analysis as punctual loads in the nodes. In this work we have considered that this stresses are created by punctual forces exerted by cells. As we are working, considering symmetries, with just a fourth of the whole geometry we fix the two symmetry faces as boundary conditions.

From the mechanical analysis it is possible to obtain the new position of the mesh nodes, that is the new geometry (deformed) of the wound and the undamaged surrounding tissue. This new geometry is introduced as the initial geometry of the next biochemical step. As

initial conditions of every biochemical step we introduce the node concentrations obtained from the last biochemical step, as they have not been modified in the mechanical analysis. In this analysis we also calculate the volumetric deformation θ that the tissue has suffered around every node and we introduce these values in the biochemical analysis to calculate the new stresses and species concentrations.

To carry out the full analysis we alternate the two analysis several times to complete the desired period. In this work we are studying a whole time period of 30 days, to compare the results against the results obtained with the biochemical model. As the biochemical evolution of the species is slower than the mechanical response we take periods of one day for the first part of the analysis while the time that we use to evaluate the mechanical behaviour is deprecated as the mechanical respond is instantaneous. We are repeating the process 30 times to complete the 30 days analysis, thus each analysis corresponds whith a day of the angiogenesis process.

3.4. Results of the complete model

In this section we present the results of the complete model in the same way as we have studied the results from the biochemical model in Section 2.4, and we compare the outcomes. Thus, we simulate a circular wound with a diameter of 2 cm and it is surrounded by a 10 cm diameter circumference of undamaged skin. We have simulated a fourth of the whole geometry as we have considered symmetry in the two axis. This wound has the same geometry as the studied in Chapter 2 so we can compare the results.

3.4.1. Comparison of the species densities in the centre of the wound

The main difference between the two cases, with and without the mechanical influence, is that in the complete model the geometry varies with time according to the deformation that the tissue suffers from the traction that the cells exert on it. First we have plotted the fibroblasts concentration in the centre of the wound (Figure 3.2). This point is the only point of the wound that does not experience any displacement due to the mechanical behaviour.

In Figure 3.2 we observe the differences between the concentration of fibroblasts in the centre of the wound when considering just biochemical factors and both biochemical and mechanical ones. At the beginning the evolution is similar in both cases, but when the mechanical factors are included, the fibroblasts density grows more rapidly due to the contraction of the wound. A possible reason is that when the mechanics is considered the boundary between the dermis and the wound is moving towards the centre of the wound, and the cellular densities are dragged in the same direction.

3.4.2. Evolution of the species densities in the whole domain

We present here the distribution of the four species densities (oxygen, macrophage-derived growth factor, capillary and fibroblasts) at day one (Figure 3.3) under the effect of cell

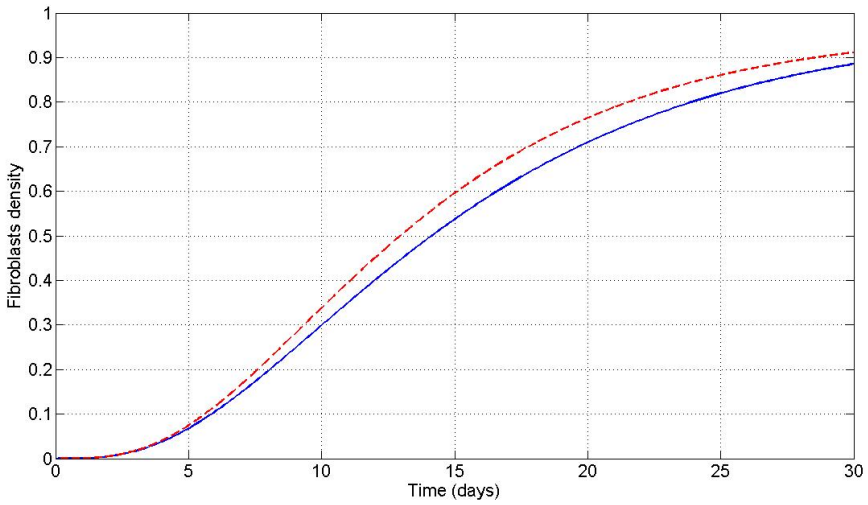

Figure 3.2: *Concentration of fibroblasts in the centre of the wound without the influence of the mechanics (blue continuous line) and with the effect of the mechanics (red dotted line).*

stresses. We observe that the concentrations are quiet similar to the ones obtained in Section 2.4.3 without the effect of the mechanics.

The different outcomes of both models could be analysed at day 30. At this time the only qualitative difference between the two models predictions is in the fibroblasts concentrations, as can be seen in Figure 3.4. The oxygen and the capillary have reached the maximal concentration in both cases and MDGF is not present in any case. The difference in the fibroblasts concentration is due mainly to the passive convection due to the contraction of the wound. When the tissue is deformed it carries the cells that are in it.

Finally, we present the geometry of the wound at day 30 post-wounding for the two cases, with and without mechanics to see how it has evolved. In the first case when only the biochemical parameters are considered, it is easy to appreciate that the mesh has not changed, but however, when the mechanical analysis has been carried out with the biochemical study the contraction of the wound is appreciable, as can be see in Figure 3.5. As a result from the stresses in the skin, the geometry of the wound modifies in time, as can be observed in a real injury.

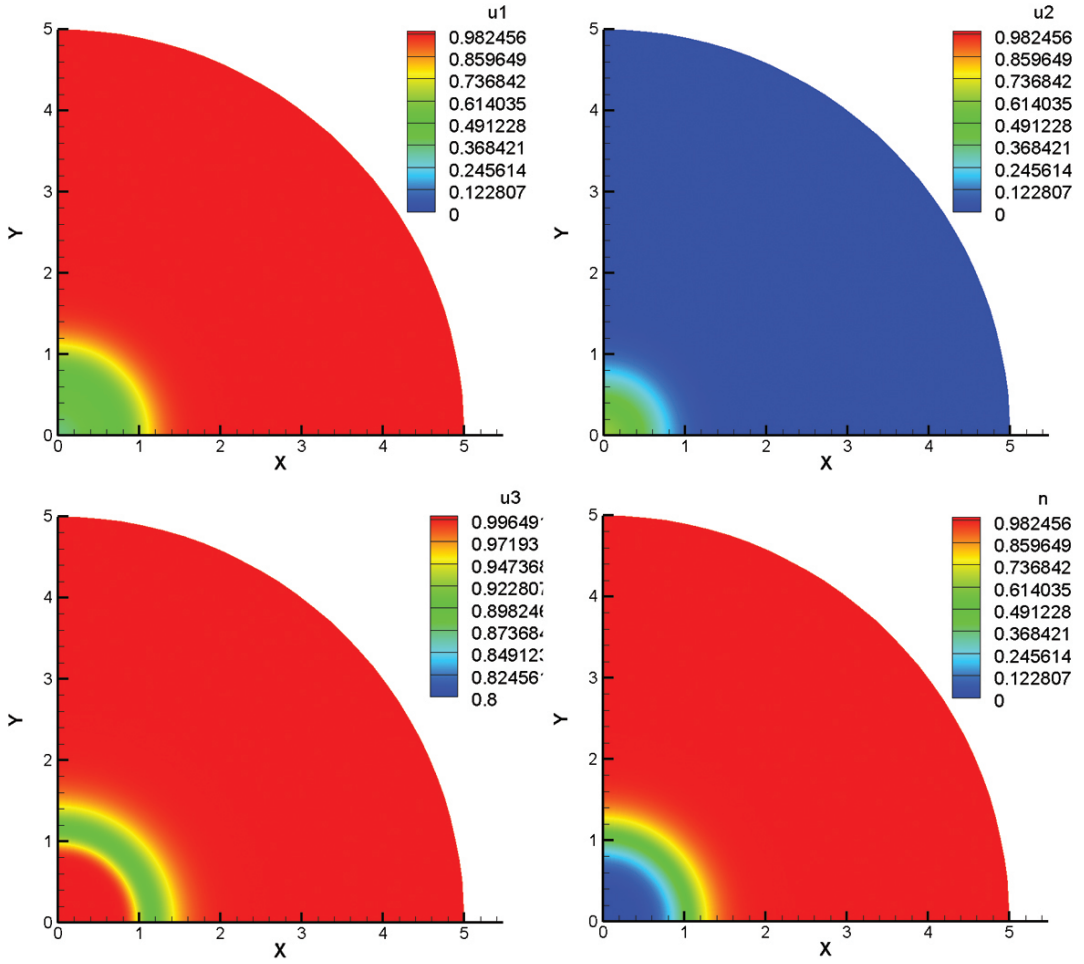

Figure 3.3: *Distribution of the four species in the whole domain at day one: oxygen (top left), MDGF (top right), capillaries (bottom left) and fibroblasts (bottom right).*

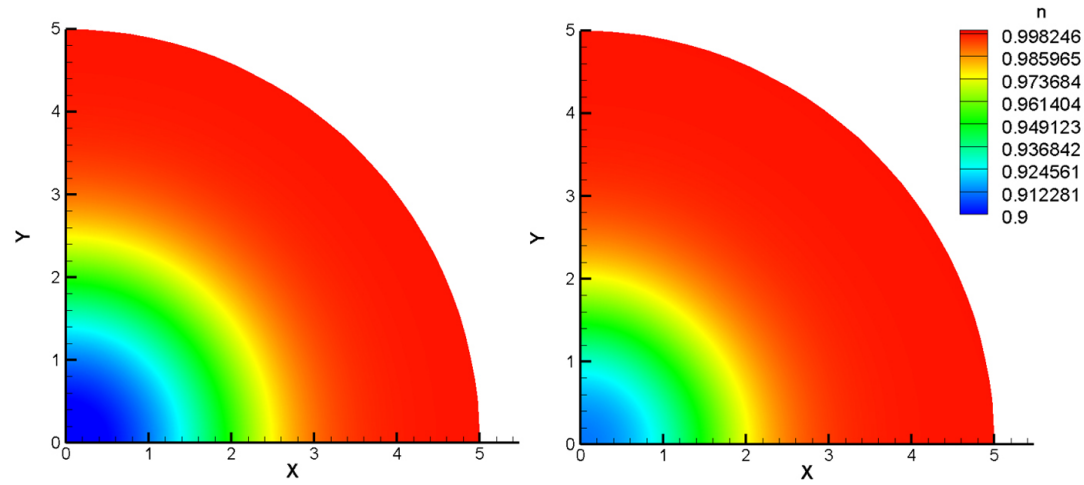

Figure 3.4: *Fibroblasts distribution in the whole domain at day 30 without the effect of the mechanics (left) and with the effect of mechanics (right).*

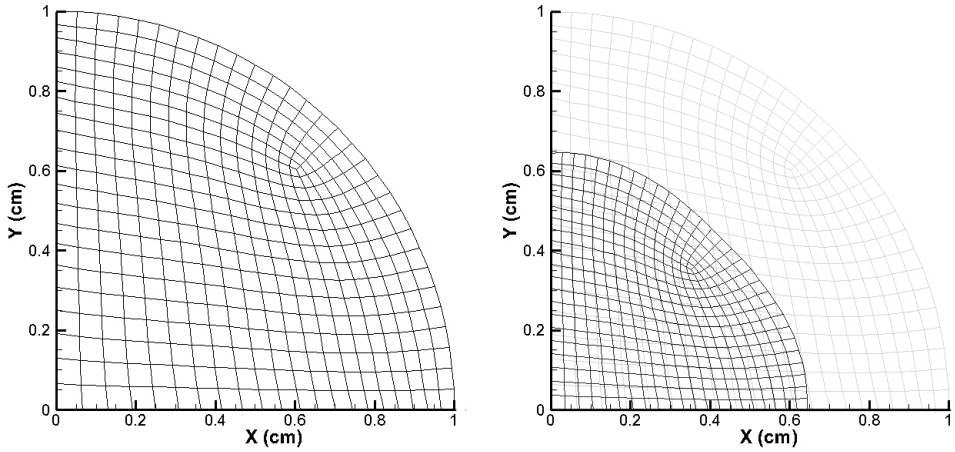

Figure 3.5: *Mesh of the wound at day 30 without the effect of the mechanics (left) and under the effect of mechanics (right).*

Chapter 4

Conclusions and future work

Wound healing is a complex process crucial in the healing of burns and traumatic and surgical wounds. This process can be divided into different phases and processes that are characterised by the presence of different cell species. Angiogenesis is one of the biological processes that take place during wound healing, and it is very important as it involves the formation of new blood vessels from the pre-existing vasculature, which allows the distribution of oxygen to the new tissue. In the last few years some numerical models that reproduce the angiogenesis process have been proposed. In this work we have presented a model that includes biological and mechanical parameters.

4.1. Conclusions

4.1.1. Conclusions from the biochemical model

In the first part of this work we have proposed a biochemical model that reproduces the angiogenesis process. First we have examined the effect of oxygen in angiogenesis. From the results, we can conclude that when oxygen is not included in the fibroblasts kinetics, the model predicts fibroblasts invasion into the wound faster than reality, and hence wound healing rate is overestimated. Therefore, the role of oxygen in the cell kinetics is a crucial factor that can not be disreagarded to model angiogenesis and wound healing accurately.

4.1.2. Conclusions from mechanobiochemical model

We have studied the effect of mechanics in the angiogenesis process. From the results we can conclude that mechanics influences the angiogenesis process due to the modification of the wound geometry. It is easy to see that the combination of biochemical and mechanical models in these kind of processes gives more information that would be lost with the use of just one model.

Results of this kind of models can help in the prescription of more appropriate healing treatments for each different wound type. These models can also help to understand unsuccessful wound healing process under certain conditions.

4.2. Future work

As it has been previously said this work is part of a project in which the complete wound healing process will be modelled and where a number of different scientific groups take part. Therefore, the main future objective is the modelling and implementation of the rest of the wound healing phases and processes. Some of these stages, as an example the contraction phase, have already been modelled by the research group. Lately, all these models will be joined in order to obtain a complete model of the whole process.

As minor objectives, there are several improvements to make in the present work. In first place, we would like to introduce the matrix density directly instead of calculating it as a function of other variables. This would give a more realistic representation of the extracellular matrix.

In addition to that, we will modify the material behaviour, adding collagen fibers to the hyperelastic material, modelling its orientation and remodelling during the angiogenesis process.

As it has been seen in Chapter 3, the cellular mechanosensing model is regulated by the value of the volumetric strain, which is a mean value of the principal strains. Therefore, a possible future improvement would be the modification of the model to regulate it by the principal strains, for example ε_{III}, which is the highest contraction strain and a maximal value, to see if the wound behaves in the same way independently of the strain that regulates the process or if its behaviour varies in each direction. It is known that the forces created by cells do not follow a isotropic distribution, but they are well directed and oriented [15].

Finally, we would like to implement the model for three-dimensional geometries, as wounds can not always be treated as two-dimensional. Some information about the process is lost with this geometric simplification as wounds do not behave in the same way in every direction.

4.3. Applications

The future applications of the model can be separated in two groups, in the biological field (medicine) and in the technological field, for the development of new materials.

4.3.1. Medical applications

Once the model will be completed, it could be applied to the study of wounds with a normal healing and to pathological wounds like ulcers, wounds caused by long inbed periods with a high mechanical influence and burns.

It is also important to notice the relevance of the model in surgery, where it can be used to determine the best place and shape of the cut to obtain the desired healing time and an appropriate contraction of the wound, as sometimes this is desired to be minimum so the resulting scar is also the smallest possible.

4.3.2. Technological applications: self-healing materials

As it has been presented in this work, nature and the skin in particular, have a self-healing ability against external damages. This ability is been studied at the moment and emulated to develop self-healing materials capable of recovering their undamaged properties. These materials are based in biomimetic principles, trying to mimic the natural healing processes.

An example of these materials is the multilayer covers, consisting on expandable materials like clay. When a crack or damage occurs, the cover absorb the humidity of the environment and begin to expand, sealing the crack. This process in an inert material is similar to the process during wound healing, as it is capable of repairing the damage; however, the recovering in inert materials is never complete, and it is not always possible for any defect size and conditions. With the complete wound healing model, a self-healing model for these type of materials could be proposed, identifying the similarities of both processes (chemical transport instead of cellular migration, chemical reactions instead of cellular synthesis, etc.).

Acknowledgements

I gratefully acknowledge research support from the Spanish Ministry of Science and Technology through the research project, Grant DPI2009-07514.

Furthermore, I also thank the Spanish Ministry of Science and Technology for the support to Clara Valero through the grant BES2010-037281.

References

[1] Cheung, J. T.-M., Zhang, M., Leung, A. K.-L., F., Y.-B., 2005. Three-dimensional finite element analysis of the foot during standing–a material sensitivity study. Journal of Biomechanics 38 1045–1054.

[2] Glazier, J.A., Graner, F., 1993. Simulation of the differential adhesion driven arrangement of biological cells. Phys Rev E 47 2128–2154.

[3] Hughes, T. J. R., 1987. The finite element method: linear static and dynamic finite element analysis. Prentice-Hall, Englewood Cliffs NJ.

[4] Javierre, E., Vermolen, F.J., Vuik, C., Zwaag, S., 2008. Numerical Modelling of Epidermal Wound Healing. In: Numerical Mathematics and Advanced Applications 83–90. Springer Berlin Heidelberg

[5] Javierre, E., Moreo, P., Doblaré, M., García-Aznar, J.M., 2009. Numerical modeling of a mechano-chemical theory for wound contraction analysis. International Journal of Solids and Structures 46 3597–3606.

[6] Lapeer, R.J., Gasson, P.D., Karri, V.,2011. A Hyperelastic Finite-Element Model of Human Skin for Interactive Real-Time Surgical Simulation. IEEE TRANSACTIONS ON BIOMEDICAL ENGINEERING 58 1013–1022.

[7] Maggelakis, S., 2003. A mathematical model of tissue replacement during epidermal wound healing. Applied Mathematical Modelling 27 189–196.

[8] Midwood, K.S., Williams, L.V., Schwarzbauer, J.E., 2004. Tissue repair and the dynamics of the extracellular matrix. International journal of biochemistry & cell biology 36 1031–1037.

[9] Moreo, P., García-Aznar, J.M., Doblaré, M., 2008. Modeling mechanosensing and its effect on the migration and proliferation of adherent cells. Acta Biomateriaalia 4 613–621.

[10] Pettet, G.J., Byrne, H.M., Mcelwain, D.L.S., Norbury, J., 1996a. A model of wound-healing angiogenesis in soft tissue. Mathematical Biosciences 136 35–63.

[11] Pettet, G., Chaplain, M.A.J., Mcelwain, D.L.S., Byrne, H.M., 1996b. On the role of angiogenesis in wound healing. Proc R Soc London Ser B 263 1487–1493.

[12] Schreml, S., Szeimies, R.M., Prantl, L., Karrer, S., Landthaler, M., Babilas, P., 2010. Oxygen in acute and chronic wound healing. British Journal of Dermatology 163 257–268.

[13] Schugart, R.C., Friedman, A., Zhao, R., Sen, C.K., 2008. Wound angiogenesis as a function of tissue oxygen tension: A mathematical model. Proc Natl Acad Sci USA 105 2628–2633.

[14] Williams, P.L., 1998. Anatomía de Gray. Volumen I. Ed. Elsevier.

[15] De, R., Zemel, A., Safran,S. A., 2007. Dynamics of cell orientation 3(9). Nature Physics 58(4) 655–659.

[16] Zienkiewicz, O. C., Taylor, R. L., 2000b. The Finite Element Method. Volume 2: Solid Mechanics. Butterworth-Heinemann, Oxford.